Eur. Phys. J. D (2021) 75:289
https://doi.org/10.1140/epjd/s10053-021-00285-3

THE EUROPEAN PHYSICAL JOURNAL D

Regular Article – Atomic and Molecular Collisions

Study of electron scattering from CH_4^+, NH_3^+, H_2O^+, NH_4^+ and H_3O^+ molecular ions with an analytic static potential approach

Dibyendu Mahato, Lalita Sharma, and Rajesh Srivastava[a]

Department of Physics, Indian Institute of Technology, Roorkee, India

Received 30 August 2021 / Accepted 2 October 2021 / Published online 17 November 2021

Abstract. A detailed study on electron impact elastic scattering from CH_4^+, NH_3^+, H_2O^+, NH_4^+ and H_3O^+ molecular ions is reported for the first time by using an optical model potential method. The static potential of each ion is obtained analytically by representing the molecular ion with Gaussian orbital wave functions. Exchange and polarization potentials are added with the static potential to form an optical model potential. Utilizing this optical model potential, the Dirac equations are solved with the partial wave phase shift analysis method to obtain the scattering amplitudes. The differential cross section results are reported for 10–500 eV incident electron energy range. These results for the different molecular ions are compared with their corresponding neutral molecules.

1 Introduction

In the present work, we address on the electron impact scattering on the ionic atomic systems. Thus, it would be interesting and worth knowing that how is the situation in general for the electron scattering from an ion. There are many possible elastic and inelastic processes when an electron interacts with an ion. There are a large number of experimental studies on electron impact excitations of atomic ions which consequently led to the development of many theoretical studies and their numerous applications [1,2]. On the other hand, there are only few experimental studies on elastic scattering of electrons from atomic ions, which gave rise to relatively less theoretical work [3–8]. If we see the literature on the similar studies of the electron impact scattering from molecular ions, we find the situation is very different and there are hardly few experimental and theoretical studies. In such scattering, there may be elastic scattering; rotational, vibrational and electronic excitations, ionization, dissociation, electron capture processes, etc. [9–17]. All these are important to understand the role of molecular ions in the study of plasma, astrophysical, atmospheric and interstellar space environments. The related cross section data of these processes are required as an input parameter in the different modeling studies. In the low-temperature plasma, at the divertor and near-wall regions of a reactor, molecules and molecular ions are formed [18]. These plasma species react with the available electrons and different molecular ions. The plasma modeling requires cross sections and rate coefficients for all these processes and spectral signatures to support the interpretation of data from fusion experiments [18]. Besides plasma applications, several atomic and molecular ions are found in space and these ions are mainly responsible for the formation of increasingly complex interstellar molecules [19]. We are now living in a molecular universe and the different species formed are from hydrogen, carbon, nitrogen and oxygen. The interstellar medium is going through several interactions with the ultraviolet radiation, energetic field and shock waves and these interactions lead to newly formed stars and planetary systems. During this evolution, simple molecules and atoms combine to form complex molecules.

In the present work, we focus our attention on the CH_4^+, NH_3^+, H_2O^+, NH_4^+ and H_3O^+ molecular ions which are mostly formed in different plasmas, astrophysical, atmospheric and interstellar space environments. For example, at the edge plasma regions methane (CH_4) is one of the major components of chemical erosion fluxes. Methane may be deliberately introduced in the divertor region for plasma diagnostic and hydrocarbon transport studies [20]. The CH_4 molecule is rapidly dissociated to a variety of neutral fragments or ionized in collisions with plasma electrons, leading to the generation of methane ions (CH_4^+). Besides the plasma applications, methane ion is noticed as an important molecular ion in the astrochemical environment of diffuse clouds, dense clouds, cometary

[a] e-mail: rajesh.srivastava@ph.iitr.ac.in (corresponding author)

comae and planetary ionosphere [21]. Most of the CH_4^+ ions are produced by interacting with the energetic particles or electromagnetic ultraviolet photons with CH_4. Also, in divertor-relevant environments, when nitrogen is puffed, ammonia is formed through Eley–Rideal and Langmuir–Hinshelwood processes, involving both volume–surface and surface–surface interactions on a (cold) metal wall. NH_3 and its protonated derivative NH_4^+ are efficient NH sources via ion conversion and recombination [22]. On the other hand, nitrogen is one of the most abundant element in the universe and its nitrogen hydrides are present in the interstellar medium and in the reaction of nitrogen ions with the H_2, it produces positive ammonium ions, i.e., NH^+, NH_2^+, NH_3^+, NH_4^+ [23]. It is noticed that in the coma of 67P/C–G near perihelion [24], NH_4^+ ion is detected as one of the most abundant ions. Likewise, H_2O is important in the international thermonuclear experimental reactor (ITER) as cooling water system to manage the heat generation during the operation of the tokamak [25]. So, there might be a possibility of the formation of some H_2O^+ and H_3O^+ molecular ions and consequently, these will have a large impact on plasma chemistry. Besides this, H_2O and its ionized forms are also very important molecules found in several areas of astronomical and atmospheric environments, e.g., the presence of $H_2O^+$is identified in the tail of comet Kohoutek [26] and H_3O^+ in Halley's comet [27].

Electron interactions with the molecular ions are getting attention due to their several applications in the plasma and astronomical studies. In this respect, various groups have been studying the electron impact inelastic processes viz. ionization, dissociation, recombination, rotational and vibrational excitation in the low incident electron energies [10,17,28,29]. There is not much attention paid on the elastic scattering of electrons from molecular ions. However, the elastic electron impact cross sections are equally important to understand the molecular properties, specially, to get the information about electron transport phenomenon in various studies. Also the depth and positions of minima in differential cross section (DCS) curves have significant physical importance as these reflect the structural information about the molecular target ion. There are only couple of theoretical studies reported on elastic electron–molecular ion scattering. These include the calculations of Lucchese and McKoy [30–32] who applied the Schwinger variational principle method to calculate the elastic electron scattering cross sections from couple of molecular ions.

In the previous work, we have successfully applied our analytically obtained static potential approach to study electron elastic and inelastic scattering cross sections from various neutral molecules [33–36]. In this method, we obtain the spherically averaged static potential by solving multicenter integrals using Gaussian orbitals centered on various atomic nuclei of the molecule. Our obtained static potential is mostly analytic except for the inclusion of the well-known error functions. Such an approach is advantageous due to available algorithms for the numerical evaluation of the error functions. Thus, the accuracy of our potentials is limited only by the accuracy of the Gaussian orbitals that are fitted to a Slater-type orbital (STO) wave function of the molecule. As the Gaussian wave functions and the obtained static potential are in the analytical form, the requirements of the memory storage are minimal. Our method produces potentials that are spherically averaged over all molecular orientations before the scattering process is carried out. In our earlier work, where possible, we have used standard and widely tested expressions of other potentials viz. exchange, polarization and absorption as components of the complex optical potential. Our optical model potential gives very accurate results at intermediate and high energy regions. In the present work, we have extended our method to a more complex problem, i.e., to study for the first time, the elastic electron scattering from the molecular ions CH_4^+, NH_3^+, H_2O^+, NH_4^+ and H_3O^+ whose importance has already been discussed above. Here also, we obtain an analytical expression for the spherically symmetric static potential of the molecular ion (seen by the projectile electron) as linear combinations of Gaussian-type molecular ionic wave functions. In addition, only exchange and polarization potentials are added to the static potential to construct the optical model potential. We have dropped the absorption potential as no suitable expression was available for the electron scattering from molecular ions. Further, we have used this potential in the Dirac equations and solved them to get the projectile electron wave function using the partial wave analysis method. The scattering phase shifts and amplitudes are calculated to find the electron impact elastic differential cross section.

Since there are no previous results available to compare with the present calculation for electron scattering from our selected CH_4^+, NH_3^+, H_2O^+, NH_4^+ and H_3O^+ molecular ions, we have also considered the electron scattering from the H_2^+ molecular ion for which theoretical results [32] are available for comparison. The comparison of our results with this available calculation will provide us the test and verification of our method.

2 Theory

2.1 Scattering amplitude and cross sections

The elastic interactions between the incident electron and the target molecular ions can be described by the spherically averaged optical model potential given by

$$V_{\rm opt}(r) = \frac{-ze^2}{r} + V_{\rm sr}(r). \tag{1}$$

Here, the first term in Eq. (1) is due to the Coulomb interaction, where e is the electronic charge and z refers to the ionic charge on the target ion. The second term $V_{\rm sr}(r)$ represents the short-range potential which includes static $V_{\rm st}(r)$, exchange $V_{\rm ex}(r)$ and polarization

$V_{\rm pol}(r)$ potentials, i.e.,

$$V_{\rm sr}(r) = V_{\rm st}(r) + V_{\rm ex}(r) + V_{\rm pol}(r). \quad (2)$$

The choices of these potentials have been discussed in detail in the following Sect. 2.2. Further, to obtain the projectile electron wave function using this optical potential, we have solved the Dirac equations following the conventional procedure for relativistic elastic scattering of electrons [37,38] and obtained the associated scattering phase shifts and amplitudes.

The relativistic incident electron wave function can be expressed as [8,38,39],

$$\psi_{{\rm E}\kappa m}(r) = \frac{1}{r}\begin{pmatrix} P_{{\rm E}\kappa}(r)\,\Omega_{\kappa,m}(\hat{\boldsymbol{r}}) \\ iQ_{{\rm E}\kappa}(r)\,\Omega_{-\kappa,m}(\hat{\boldsymbol{r}}) \end{pmatrix}, \quad (3)$$

where $\Omega_{\kappa,m}(\hat{\boldsymbol{r}})$ are the spherical spinors, κ is the relativistic quantum number, which is defined as $\kappa = (l-j)(2j+1)$, where l and j are the orbital and total angular momentum quantum numbers that are both determined by the value of κ as $j = |\kappa| - 1/2$, $l = j + \kappa/(2|\kappa|)$. $P_{{\rm E}\kappa}$ and $Q_{{\rm E}\kappa}$ are, respectively, the large and small component of the radial wavefunction of the projectile electron and satisfy the following coupled Dirac equations

$$\frac{{\rm d}P_{{\rm E}\kappa}(r)}{{\rm d}r} = -\frac{\kappa}{r}P_{{\rm E}\kappa}(r) + \frac{E - V_{\rm opt} - 2m_{\rm e}c^2}{c\hbar}Q_{{\rm E}\kappa}(r) \quad (4)$$

$$\frac{{\rm d}Q_{{\rm E}\kappa}}{{\rm d}r} = -\frac{E - V_{\rm opt}}{c\hbar}P_{{\rm E}\kappa}(r) + \frac{\kappa}{r}Q_{{\rm E}\kappa}(r). \quad (5)$$

Here, E represents the incident electron energy, $m_{\rm e}$ is the rest mass of the electron, c is the velocity of light in vacuum and $\hbar$ is the Planck's constant. Now if we expand the total wavefunction equation (3) into its relativistic form of the partial wave expansion, we obtain the solutions by using the following asymptotic ($r \to \infty$) boundary conditions

$$P_{{\rm E}\kappa}(r) \sim \sin\left(kr - l\frac{\pi}{2} - \eta{\rm ln}2kr + \delta_k\right) \quad (6)$$

$$Q_{{\rm E}\kappa}(r) \sim \cos\left(kr - l\frac{\pi}{2} - \eta{\rm ln}2kr + \delta_k\right). \quad (7)$$

Here, k is the relativistic momentum of the projectile electron and η is the Sommerfeld parameter given by

$$\eta = \frac{ze^2 m_{\rm e}}{\hbar k}. \quad (8)$$

In Eqs. (6) and (7), δ_k is the total phase shift which is the sum of the phase shifts resulting from the short-range potential ($\hat{\delta}_\kappa$) and the Coulomb phase shift (Δ_κ) due to the ionic charge z, i.e., $\delta_k = \hat{\delta}_\kappa + \Delta_\kappa$.

Thus, in the presence of the Coulomb and short-range potentials, the direct and spin–flip scattering amplitudes can be expressed as,

$$f(\theta) = f_{\rm sr}(\theta) + f^{(C)}(\theta) \ \text{ and } \ g(\theta) = g_{\rm sr}(\theta) + g^{(C)}(\theta). \quad (9)$$

Here, $f_{\rm sr}(\theta)$ and $g_{\rm sr}(\theta)$ are the scattering amplitude contributions due to the short-range part of the potential as given bellow

$$f_{\rm sr}(\theta) = \frac{1}{2ik}\sum_{l=0}^{\infty}\{(l+1)\exp(2i\Delta_{-l-1}) \times \left[\exp\left(2i\hat{\delta}_{-l-1}\right) - 1\right] + l\ \exp(2i\Delta_l)\left[\exp\left(2i\hat{\delta}_l\right) - 1\right]\}P_l(\cos\theta), \quad (10)$$

and

$$g_{\rm sr}(\theta) = \frac{1}{2ik}\sum_{l=0}^{\infty}\left\{\exp(2i\Delta_l)\left[\exp\left(2i\hat{\delta}_l\right) - 1\right] - \exp(2i\Delta_{-l-1})\left[\exp\left(2i\hat{\delta}_{-l-1}\right) - 1\right]\right\}P_l^1(\cos\theta). \quad (11)$$

Also, the scattering amplitude contribution for the Coulomb interaction with z, $f^{(C)}(\theta)$ and $g^{(C)}(\theta)$ can be expressed as

$$f^{(C)}(\theta) = \frac{1}{2ik}\sum_{l=0}^{\infty}\{(l+1)[\exp(2i\Delta_{-l-1}) - 1] + l\,[\exp(2i\Delta_l) - 1]\}P_l(\cos\theta), \quad (12)$$

and

$$g^{(C)}(\theta) = \frac{1}{2ik}\sum_{l=0}^{\infty}\{\exp(2i\Delta_l) - \exp(2i\Delta_{-l-1})\}P_l^1(\cos\theta). \quad (13)$$

Further using Eq. (9), we can calculate the required DCS as

$$\frac{{\rm d}\sigma}{{\rm d}\Omega} = |f(\theta)|^2 + |g(\theta)|^2. \quad (14)$$

2.2 Optical model potential

The electronic static potential $V(r)$ for the molecular ions as seen by the projectile electron at a point $\boldsymbol{r}$, can be represented by

$$V(r) = \int \frac{\rho(\boldsymbol{r}')}{|\boldsymbol{r} - \mathbf{r}'|}{\rm d}\mathbf{r}'. \quad (15)$$

Considering the molecular orbitals to be orthogonal, the charge density at a point $\boldsymbol{r}'$ in the above expression

can be represented by

$$\rho\left(\boldsymbol{r}'\right)=\sum_{i=1}^{N}\left|X_i\left(\boldsymbol{r}'\right)\right|^2, \tag{16}$$

where X_i is the molecular wave function and the index i goes up to the number of molecular orbitals, which are 5 alpha electrons and 4 beta electrons for CH_4^+, NH_3^+, H_2O^+ and 5 for NH_4^+, H_3O^+. The molecular orbitals $X_i\left(\boldsymbol{r}'\right)$ are further expressed as a linear combination of atomic orbitals $\phi_k(\boldsymbol{r}')$, i.e.,

$$X_i\left(\boldsymbol{r}'\right)=\sum_k a_{ik}\phi_k\left(\boldsymbol{r}'\right), \tag{17}$$

where a_{ik} is the molecular orbital coefficient and k extends on the total number of atomic orbitals which are 9 for CH_4^+, 8 for NH_3^+, 7 for H_2O^+, 9 for NH_4^+ and 8 for H_3O^+. Each atomic orbital is represented as

$$\phi_k\left(\boldsymbol{r}'\right)=\sum_j N_{kj}c_{kj}\chi_{kj}(\boldsymbol{r}'), \tag{18}$$

where N_{kj} are normalization constants and c_{kj} are the coefficients of the Gaussian basis functions $\chi_{kj}(\boldsymbol{r}')$. The sum over j denotes the number of Gaussian basis functions which is taken 6 in the present calculations. The unnormalized form of the Gaussian basis functions $\chi_{kj}(\boldsymbol{r}')$ which are centered on the nucleus at A with coordinates A_x, A_y and A_z is represented as

$$\begin{aligned}\chi_{kj}\left(\boldsymbol{r}'\right)=\;& e^{-\alpha_{kj}\left|\boldsymbol{r}'-\boldsymbol{A}\right|^2}\left(x'-A_x\right)^{m_x}\\ &\times\left(y'-A_y\right)^{m_y}\left(z'-A_z\right)^{m_z}.\end{aligned} \tag{19}$$

Here, m_x, m_y and m_z are nonnegative integers and α_{kj} is the exponents of the Gaussian basis function.

The molecular orbitals are further expressed in terms of the linear combination of the Gaussian atomic orbitals. Thus, the charge density can be expressed as,

$$\begin{aligned}\rho\left(\mathbf{r}'\right)=\;&\sum_i\sum_{k,k'}a_{ik}a_{ik'}\\ &\times\sum_{j,j'}N_{kj}N_{k'j'}c_{kj}c_{k'j'}\chi_{kj}(\boldsymbol{r}')\chi_{k'j'}(\boldsymbol{r}').\end{aligned} \tag{20}$$

The Gaussian orbitals have a very important property that the product of the exponential parts of two orbitals with different centers **A** and **B** can be written as an exponential of the same form at a center P on the line joining **A** and **B**. Thus, the product of two Gaussian functions in Eq. (20) becomes

$$\begin{aligned}\chi_{kj}\left(\boldsymbol{r}'\right)\chi_{k'j'}\left(\boldsymbol{r}'\right)&=e^{-\alpha_{kj}\left|r'-\boldsymbol{A}\right|^2}e^{-\alpha_{k'j'}\left|r'-\boldsymbol{B}\right|^2}\\ &\times\left(x'-A_x\right)^{m_x}\left(y'-A_y\right)^{m_y}\left(z'-A_z\right)^{m_z}\\ &\times\left(x'-B_x\right)^{m_x'}\left(y'-B_y\right)^{m_y'}\left(z'-B_z\right)^{m_z'}\\ &=E_{kj,k'j'}e^{-\alpha\left|r'-\boldsymbol{r}_P\right|^2}\left(x'-A_x\right)^{m_x}\\ &\times\left(y'-A_y\right)^{m_y}\left(z'-A_z\right)^{m_z}\\ &\times\left(x'-B_x\right)^{m_x'}\left(y'-B_y\right)^{m_y'}\left(z'-B_z\right)^{m_z'},\end{aligned} \tag{21}$$

where $\boldsymbol{r}_P$ is the position vector of P with respect to the molecular frame can be given by

$$\begin{aligned}\boldsymbol{r}_P&=\frac{\alpha_{kj}\mathbf{A}+\alpha_{k'j'}\mathbf{B}}{\alpha_{kj}+\alpha_{k'j'}},\\ \alpha&=\left(\alpha_{kj}+\alpha_{k'j'}\right)\text{ and}\\ E_{kj,k'j'}&=e^{\left(-\frac{\alpha_{kj}\alpha_{k'j'}}{\alpha_{kj}+\alpha_{k'j'}}|\mathbf{A}-\mathbf{B}|^2\right)}.\end{aligned}$$

Here, $\boldsymbol{r}_P$ is the position vector at P and $E_{kj,k'j'}$ refers to the coefficients when two Gaussian exponentials have been multiplied with two different centers **A** and **B**.

Further, using Eq. (21) and substituting the charge density in Eq. (15) and expanding the denominator using the property of spherical harmonics, we get the spherically averaged static electronic potential over all the orientations of the molecule,

$$\begin{aligned}V(r)=&\sum_i\sum_{k,k'}a_{ik}a_{ik'}\sum_{j,j'}N_{kj}N_{k'j'}c_{kj}c_{k'j'}E_{kj,k'j'}\\ &\times\int e^{-\alpha\left|r'-r_p\right|^2}\left(x'-A_x\right)^{m_x}\left(y'-A_y\right)^{m_y}\left(z'-A_z\right)^{m_z}\\ &\times\left(x'-B_x\right)^{m_x'}\left(y'-B_y\right)^{m_y'}\left(z'-B_z\right)^{m_z'}\frac{1}{r_>}\mathrm{d}\mathbf{r}'.\end{aligned} \tag{22}$$

Here, $r_>$ is greater of r and r'. These integrals in the above equation are further evaluated by considering the multiplications of the two different atomic Gaussian orbitals, i.e., two s-orbital of hydrogen atoms ($1s$) or say atom X [i.e., C ($1s^22s^22p^2$), N ($1s^22s^22p^3$) or O ($1s^22s^22p^4$)], s-orbital of hydrogen (H) atom with the p-orbital of atom X or two p-orbitals of atom X. A detailed description of the occurring integrals for the interactions of s–s, s–p and p–p orbitals and their evaluation in terms of known error functions are given in our previous paper [40]. We have evaluated Eq. (22) in a particular molecular frame of reference and this has been further discussed fully in the forthcoming Sect. 3 on results and discussion.

Along with the electronic static potential $V(r)$, we also have to include the effective nuclear potential $V_{\mathrm{nucl}}(r)$ seen by the projectile electron. It can be

expressed as

$$V_{\text{nucl}}(r) = -\sum_n \frac{Z_{H_n}}{|\boldsymbol{r} - \boldsymbol{r}_{H_n}|} - \frac{Z_X}{|\boldsymbol{r} - \boldsymbol{r}_X|}. \quad (23)$$

Here, Z_X (X represents either C or N or O atom of the molecular ions CH_4^+, NH_3^+, H_2O^+, NH_4^+ and H_3O^+) and Z_{H_n} (n refers to the different H atoms of the corresponding molecular ions) are the atomic numbers of X and H atom, respectively. Also, $\boldsymbol{r}_{H_n}$ and $\boldsymbol{r}_X$, respectively, represent the position vectors of hydrogen and X atoms from the center of their original axes, i.e., the center of mass of the molecule. It is important to note that the absolute value of the position vector r_H for all the three hydrogen atoms in the molecule are the same because of the symmetry of the molecular structure. Taking the spherical average of the nuclear terms [41,42] in Eq. (23) and including the spherically averaged static potential $V(r)$ for the electrons distribution of the molecule, we can express the total spherically averaged static potential for each molecule as

$$V_{\text{st}}(r) = V(r) - \frac{nZ_H}{r''_>} - \frac{Z_X}{r'''_>}. \quad (24)$$

Here, $r''_>$ is maximum of (r, r_H) and $r'''_>$ is maximum of (r, r_X). Thus, the total static potential from Eq. (24) can further be rewritten to describe the elastic electron scattering from H_2^+, CH_4^+, NH_3^+, H_2O^+, NH_4^+ and H_3O^+ as

$$V_{\text{st}}(r) = \begin{cases} V(r) - \frac{nZ_H}{r} - \frac{Z_X}{r} \text{ for } r \geq r_H \\ V(r) - \frac{nZ_H}{r_H} - \frac{Z_X}{r} \text{ for } r_X < r < r_H \\ V(r) - \frac{nZ_H}{r_H} - \frac{Z_X}{r_X} \text{ for } r \leq r_X. \end{cases} \quad (25)$$

The molecular ions for which the core atom is situated at the center of mass, i.e., for NH_3^+ and NH_4^+, the total static potential can be expressed as,

$$V_{\text{st}}(r) = \begin{cases} V(r) - \frac{nZ_H}{r} - \frac{Z_X}{r} \text{ for } r \geq r_H \\ V(r) - \frac{nZ_H}{r_H} - \frac{Z_X}{r} \text{ for } r < r_H \end{cases} \quad (26)$$

In our calculations, we have taken the values of $r_H = 1.1142$ and $r_X = 0.1036$ for CH_4^+, $r_H = 1.0247$ for NH_3^+, $r_H = 1.0242$ for NH_4^+, $r_H = 0.9440$ and $r_X = 0.1158$ for H_2O^+, $r_H = 0.9625$ and $r_X = 0.0729$ for H_3O^+ in Å.

In the present calculation, we have used the exchange potential as given by Furness–McCarthy [43]

$$V_{\text{ex}} = \frac{1}{2}\{E - V_{\text{st}}(r)\} - \frac{1}{2}\left[\{E - V_{\text{st}}(r)\}^2 + 4\pi\rho(r)\right]^2. \quad (27)$$

Here, E is the incident electron energy and a_0 is the Bohr radius. We have also included Buckingham-type polarization potential which can be expressed as,

$$V_{\text{pol}}(r) = -\frac{\alpha_{\text{d}}}{2r^4}, \quad (28)$$

where α_{d} is the dipole polarizability of the target ion. We have taken only the asymptotic form of the polarization potential as for the electron–ion scattering, Coulomb potential is dominant and hence, short-range correlation part of polarization is neglected.

As mentioned above, all the different parts of the optical potential (1) are obtained in the analytical form and then used in the Dirac equations which are solved using the partial wave phase shift analysis [8,38,39] method and the boundary conditions (Eqs. 6 and 7) to obtain the phase shifts. The problem is solved separately for the Coulomb and short-range potentials, with which the scattering amplitudes $f(\theta)$ and $g(\theta)$ in Eq. (9) are calculated and then the cross section results are obtained using Eq. (14) for CH_4^+, NH_3^+, NH_4^+, H_2O^+ and H_3O^+ molecular ions. These results are presented and discussed in the next section.

Since, we are considering the electron scattering from an ionic system which involves the Coulomb potential, the scattering amplitudes represented in Eqs. (10–13) may give rise to convergence problems in the partial wave expansion of the scattering amplitudes. Also, for the ionic species, such as NH_3^+, H_2O^+ and H_3O^+ are having permanent dipole moment may require higher partial waves for the convergence of the scattering amplitudes. It is worth mentioning here that in the present work, the computer code we have used can take as many as over 500–600 partial waves without any problem and thus take care of any convergence problem in the summation over the partial waves of the scattering amplitudes. In fact, we have achieved the sufficient convergence (0.001%) for our results of these above ions by including 350 partial waves at the maximum incident electron energy.

3 Results and discussion

Through the GAUSSIAN-16 software, we have evaluated the analytical form of the Gaussian wavefunction of CH_4^+, NH_3^+, H_2O^+, NH_4^+ and H_3O^+ with STO-6G Gaussian basis set. We also obtained simultaneously the coefficients a_{ik} and c_{kj} and exponents α_{kj} as in Eqs. (17), (18) and (19) and their corresponding values are given in Tables 1, 2, 3, 4, 5, 6, 7 and 8. Further, using the B3LYP/CC-PVTZ basis set, we obtained the dipole polarizability values for CH_4^+, NH_3^+, H_2O^+, NH_4^+ and H_3O^+ which are given in Table 9.

Further, we have solved the integral given in Eq. (22) in a molecular frame of reference, e.g., CH_4^+ is fixed with the C atom at (0.0000, 0.0000, 0.1036) and the four H atoms at the positions (0.0000, 0.9529, 0.6179), (0.0000, −0.9529, 0.6179), (0.5761, 0.0000, −0.9286)

Table 1 Energy eigenvalues of the molecular orbitals of CH_4^+ with the coefficients a_{ik} as in Eq. (17)

Energy eigenvalues (eV)		Alpha electrons					Beta electrons			
		−11.64776	−1.35926	−0.98255	−0.93119	−0.84550	−11.63027	−1.24801	−0.94419	−0.91550
C	$1s$	0.99514	−0.20971	−0.07849	0.00000	0.00000	0.99574	−0.20433	−0.05945	0.00000
	$2s$	0.02328	0.66091	0.30316	0.00000	0.00000	0.02053	0.62408	0.21385	0.00000
	$2p_x$	0.00000	0.00000	0.00000	0.00000	0.74612	0.00000	0.00000	0.00000	0.00000
	$2p_y$	0.00000	0.00000	0.00000	0.66185	0.00000	0.00000	0.00000	0.00000	0.62261
	$2p_z$	−0.00183	−0.11725	0.51380	0.00000	0.00000	−0.00178	−0.11395	0.52353	0.00000
H1	$1s$	−0.00429	0.10965	0.24782	0.33597	0.00000	−0.00368	0.15974	0.27058	0.36818
H2	$1s$	−0.00429	0.10965	0.24782	−0.33597	0.00000	−0.00368	0.15974	0.27058	−0.36818
H3	$1s$	−0.00364	0.20880	−0.30122	0.00000	0.40155	−0.00342	0.19714	−0.29239	0.00000
H4	$1s$	−0.00364	0.20880	−0.30122	0.00000	−0.40155	−0.00342	0.19714	−0.29239	0.00000

Table 2 Energy eigenvalues of the molecular orbitals of NH_3^+ with the coefficients a_{ik} as in Eq. (17)

Energy eigenvalues (eV)		Alpha electrons					Beta electrons			
		−16.12610	−1.60089	−1.06909	−1.06909	−0.94230	−16.09334	−1.44846	−1.03398	−1.03398
N	$1s$	0.99598	−0.23008	0.00000	0.00000	0.00000	0.99668	−0.21424	0.00000	0.00000
	$2s$	0.02018	0.87334	0.00000	0.00000	0.00000	0.01676	0.77115	0.00000	0.00000
	$2p_x$	0.00000	0.00000	0.00000	0.71790	0.00000	0.00000	0.00000	0.00000	0.66170
	$2p_y$	0.00000	0.00000	0.71790	0.00000	0.00000	0.00000	0.00000	0.66170	0.00000
	$2p_z$	0.00000	0.00000	0.00000	0.00000	1.00000	0.00000	0.00000	0.00000	0.00000
H1	$1s$	−0.00411	0.09650	0.35238	0.00000	0.00000	−0.00340	0.15503	0.40946	0.00000
H2	$1s$	−0.00411	0.09650	−0.17619	−0.30517	0.00000	−0.00340	0.15503	−0.20473	−0.35461
H3	$1s$	−0.00411	0.09650	−0.17619	0.30517	0.00000	−0.00340	0.15503	−0.20473	0.35461

Table 3 Energy eigenvalues of the molecular orbitals of H_2O^+ with the coefficients a_{ik} as in Eq. (17)

Energy eigenvalues (eV)		Alpha electrons					Beta electrons			
		−21.27055	−1.89650	−1.17374	−1.09983	−1.04427	−21.23826	−1.72119	−1.13078	−0.98505
O	$1s$	0.99664	−0.23498	0.00000	0.00000	−0.07157	0.99719	−0.22351	0.00000	−0.08366
	$2s$	0.01567	0.93137	0.00000	0.00000	0.38076	0.01316	0.86847	0.00000	0.43924
	$2p_x$	0.00000	0.00000	0.00000	1.00000	0.00000	0.00000	0.00000	0.00000	0.00000
	$2p_y$	0.00000	0.00000	0.74397	0.00000	0.00000	0.00000	0.00000	0.69459	0.00000
	$2p_z$	−0.00272	−0.15036	0.00000	0.00000	0.87181	−0.00243	−0.15412	0.00000	0.85073
H1	$1s$	−0.00345	0.08048	0.31583	0.00000	−0.18829	−0.00293	0.13363	0.36261	−0.20302
H2	$1s$	−0.00345	0.08048	−0.31583	0.00000	−0.18829	−0.00293	0.13363	−0.36261	−0.20302

Table 4 Energy eigenvalues of the molecular orbitals of NH_4^+ with the coefficients a_{ik} as in Eq. (17)

Energy eigenvalues (eV)		−16.05751	−1.55539	−1.00842	−1.00842	−1.00842
N	$1s$	0.99602	−0.22095	0.00000	0.00000	0.00000
	$2s$	0.02071	0.80675	0.00000	0.00000	0.00000
	$2p_x$	0.00000	0.00000	0.00000	0.00000	0.69573
	$2p_y$	0.00000	0.00000	0.00000	0.69573	0.00000
	$2p_z$	0.00000	0.00000	0.69573	0.00000	0.00000
H1	$1s$	−0.00373	0.10304	0.23858	0.23858	0.23858
H2	$1s$	−0.00373	0.10304	0.23858	−0.23858	−0.23858
H3	$1s$	−0.00373	0.10304	−0.23858	0.23858	−0.23858
H4	$1s$	−0.00373	0.10304	−0.23858	−0.23858	0.23858

Table 5 Energy eigenvalues of the molecular orbitals of H_3O^+ with the coefficients a_{ik} as in Eq. (17)

Energy eigenvalues (eV)		−21.11860	−1.79183	−1.10556	−1.10556	−0.91836
O	$1s$	0.99659	−0.22791	0.00000	0.00000	−0.05120
	$2s$	0.01651	0.87416	0.00000	0.00000	0.26991
	$2p_x$	0.00000	0.00000	0.70884	0.00000	0.00000
	$2p_y$	0.00000	0.00000	0.00000	0.70884	0.00000
	$2p_z$	−0.00189	−0.10491	0.00000	0.00000	0.95600
H1	$1s$	−0.00310	0.09400	0.00000	0.39625	−0.08002
H2	$1s$	−0.00310	0.09400	−0.34316	−0.19812	−0.08002
H3	$1s$	−0.00310	0.09400	0.34316	−0.19812	−0.08002

Table 6 Calculated values of exponents α_{kj} and coefficients c_{kj} of STO-6G orbitals of CH_4^+

CH_4^+			
Atom	Orbital	Exponent	Coefficient
C	$1s$	0.7427370491E+03	0.9163596281E–02
		0.1361800249E+03	0.4936149294E–01
		0.3809826352E+02	0.1685383049E+00
		0.1308778177E+02	0.3705627997E+00
		0.5082368648E+01	0.4164915298E+00
		0.2093200076E+01	0.1303340841E+00
	$2s$	0.3049723950E+02	− 0.1325278809E–01
		0.6036199601E+01	− 0.4699171014E–01
		0.1876046337E+01	− 0.3378537151E–01
		0.7217826470E+00	0.2502417861E+00
		0.3134706954E+00	0.5951172526E+00
		0.1436865550E+00	0.2407061763E+00
	$2p_x$,	0.3049723950E+02	0.3759696623E–02
	$2p_y$,	0.6036199601E+01	0.3767936984E–01
	$2p_z$	0.1876046337E+01	0.1738967435E+00
		0.7217826470E+00	0.4180364347E+00
		0.3134706954E+00	0.4258595477E+00
		0.1436865550E+00	0.1017082955E+00
H	$1s$	0.3552322122E+02	0.9163596281E–02
		0.6513143725E+01	0.4936149294E–01
		0.1822142904E+01	0.1685383049E+00
		0.6259552659E+00	0.3705627997E+00
		0.2430767471E+00	0.4164915298E+00
		0.1001124280E+00	0.1303340841E+00

and (− 0.5761, 0.0000, − 0.9286); for NH_3^+, N is centered at (0.0000, 0.0000, 0.0000) and three H atoms are at (0.0000, 1.0247, 0.0000), (− 0.8874, − 0.5123, 0.0000) and (0.8874, − 0.5123, 00000) and for H_2O^+, O is centered at (0.0000, 0.0000, 0.11582) and two H atoms at (0.0000, 0.82253, − 0.46329) and (0.0000, − 0.82253, − 0.46329). Similarly for NH_4^+, the position of N is situated at (0.0000, 0.0000, 0.0000) and the four H atoms are at the positions (0.59126, 0.59126, 0.59126), (− 0.59126, − 0.59126, 0.59126), (− 0.59126, 0.59126, − 0.59126), (0.59126, − 0.59126, − 0.59126); for H_3O^+, O is centered at (0.0000, 0.0000, 0.07299) with the three H atoms at (0.0000, 0.94264, − 0.19463), (− 0.81635, − 0.47132, − 0.19463) and (0.81635, − 0.47132, − 0.19463). In Eq. (22), $\boldsymbol{r}_P$ is the product vector of the wavefunctions for H with X (where X = C, N, O) or two H atoms. In order to coincide the $\boldsymbol{r}_P$ vector with the molecular frame as given in Fig. 1, one must rotate $\boldsymbol{r}_P$ frame through Euler angles (α, β, γ). Here, we take $\boldsymbol{r}_P$ vector to be along the z_P axis in the r_P frame. This choice makes it possible to have the angle $\alpha = 0$, which leads to significant simplifications in our geometrical considerations. Further, the direction of y_p is decided by the cross product $\boldsymbol{r}_P \times z$ and the remaining axis x_p is specified to complete the standard coordinate axes. If we consider the angle between $\boldsymbol{r}_P$ and the original z-axis to be β, then, at first, y_p axis is rotated by an angle β [$0 \leq \beta \leq \pi$] to bring $\boldsymbol{r}_P$ into the z-axis. Subsequently, the z-axis is rotated through angle γ so that y_p coincides with the y-axis of the original molecular frame. The obtained values of the Euler angles for CH_4^+, NH_3^+, H_2O^+, NH_4^+ and H_3O^+ are given in Table 10.

After evaluating the static potential in Eq. (22), we construct the optical potential in Eq. (1). Thereafter, the Dirac equations are solved using partial wave anal-

Table 7 Calculated values of exponents α_{kj} and coefficients c_{kj} of STO-6G orbitals of NH_3^+ and NH_4^+

NH_3^+ and NH_4^+			
Atom	Orbital	Exponent	Coefficient
N	$1s$	0.1027828458E+04	0.9163596281E–02
		0.1884512226E+03	0.4936149294E–01
		0.5272186097E+02	0.1685383049E+00
		0.1811138217E+02	0.3705627997E+00
		0.7033179691E+01	0.4164915298E+00
		0.2896651794E+01	0.1303340841E+00
	$2s$	0.3919880787E+02	− 0.1325278809E–01
		0.7758467071E+01	− 0.4699171014E–01
		0.2411325783E+01	− 0.3378537151E–01
		0.9277239437E+00	0.2502417861E+00
		0.4029111410E+00	0.5951172526E+00
		0.1846836552E+00	0.2407061763E+00
	$2p_x$,	0.3919880787E+02	0.3759696623E–02
	$2p_y$,	0.7758467071E+01	0.3767936984E–01
	$2p_z$	0.2411325783E+01	0.1738967435E+00
		0.9277239437E+00	0.4180364347E+00
		0.4029111410E+00	0.4258595477E+00
		0.1846836552E+00	0.1017082955E+00
H	$1s$	0.3552322122E+02	0.9163596281E–02
		0.6513143725E+01	0.4936149294E–01
		0.1822142904E+01	0.1685383049E+00
		0.6259552659E+00	0.3705627997E+00
		0.2430767471E+00	0.4164915298E+00
		0.1001124280E+00	0.1303340841E+00

Table 8 Calculated values of exponents α_{kj} and coefficients c_{kj} of STO-6G orbitals of H_2O^+ and H_3O^+

H_2O^+ and H_3O^+			
Atom	Orbital	Exponent	Coefficient
O	$1s$	0.1355584234E+04	0.9163596281E–02
		0.2485448855E+03	0.4936149294E–01
		0.6953390229E+02	0.1685383049E+00
		0.2388677211E+02	0.3705627997E+00
		0.9275932609E+01	0.4164915298E+00
		0.3820341298E+01	0.1303340841E+00
	$2s$	0.5218776196E+02	− 0.1325278809E–01
		0.1032932006E+02	− 0.4699171014E–01
		0.3210344977E+01	− 0.3378537151E–01
		0.1235135428E+01	0.2502417861E+00
		0.5364201581E+00	0.5951172526E+00
		0.2458806060E+00	0.2407061763E+00
	$2p_x$,	0.5218776196E+02	0.3759696623E–02
	$2p_y$,	0.1032932006E+02	0.3767936984E–01
	$2p_z$	0.3210344977E+01	0.1738967435E+00
		0.1235135428E+01	0.4180364347E+00
		0.5364201581E+00	0.4258595477E+00
		0.2458806060E+00	0.1017082955E+00
H	$1s$	0.3552322122E+02	0.9163596281E–02
		0.6513143725E+01	0.4936149294E–01
		0.1822142904E+01	0.1685383049E+00
		0.6259552659E+00	0.3705627997E+00
		0.2430767471E+00	0.4164915298E+00
		0.1001124280E+00	0.1303340841E+00

Table 9 Calculated polarizability (Å^3) of CH_4^+, NH_3^+, H_2O^+, NH_4^+ and H_3O^+ molecular ions

Molecular ion	Polarizability
CH_4^+	1.6880
NH_3^+	1.0341
H_2O^+	0.7266
NH_4^+	1.2889
H_3O^+	0.8957

ysis and phase shifts are evaluated as explained earlier. We compute the scattering amplitudes (Eqs. 9–11) and calculate differential cross sections for elastic scattering of electrons from CH_4^+, NH_3^+, H_2O^+, NH_4^+ and H_3O^+ molecular ions.

3.1 DCS results for electron–CH_4^+ scattering

We have calculated the DCS results for the electron scattering from CH_4^+, NH_3^+, H_2O^+, NH_4^+ and H_3O^+. As already mentioned earlier that there are no earlier reported results for CH_4^+, NH_3^+, H_2O^+, NH_4^+ and H_3O^+ with which we can compare our calculated cross sections in the present work. Therefore, applying our present theory, we have also performed the calculation for a straightforward case of electron–H_2^+ for which theoretical results reported by Lucchese and McKoy [32] are available for comparison and we can test our method and verify our results. In Fig. 2, we have shown our DCS results for electron–H_2^+ scattering as compared with the calculation of Lucchese and McKoy [32] available at incident electron energy of 13.6 eV. We observe from this figure that both, ours and their calculations show reasonably good agreement. This little difference in both the calculations may be due to the different theoretical approaches used as we have used the model potential method while Lucchese and McKoy [32] used the Schwinger variational principle method. In Fig. 2, we have also shown our Coulomb scattering results to see the effect of Coulomb potential only. Comparing our DCS with the Coulomb scattering results, we find that the Coulomb potential dominates up to 120° of the scattering angles and thereafter short-range part of the potential contributes at this particular incident electron energy of 13.6 eV.

We have presented all our electron impact elastic DCS results for the different molecular ions viz. CH_4^+, NH_3^+, H_2O^+, NH_4^+ and H_3O^+, respectively, in Figs. 3, 5, 7, 9 and 10 in the entire scattering angle range of 0–180° at different incident electron energies. We have also presented the comparison of DCS results for the molecular ions CH_4^+, NH_3^+ and H_2O^+ with their corresponding neutral molecules, respectively, in Figs. 4, 6 and 8. The DCS results for the neutral molecules are those which we reported through our earlier publications [33,34,40]. Unfortunately, there are no DCS results available for the NH_4 and H_3O with which we could compare our presently calculated results for NH_4^+ and H_3O^+ ions. Further, we have also included in Figs. 4, 6 and 8, for comparison purposes, the DCS contribution corresponding to the part of the Coulomb scattering amplitude alone. This will provide us a separate contribution coming to the DCS from the scattering of the Coulomb potential only.

The present DCS results for CH_4^+ are shown in Fig. 3 for the incident electron energy range from 10 to 50 eV. We can see from Fig. 3a that in the forward direction, the DCS values are very high and as the scattering angle increases, the cross sections fall off with and without showing structures (minima and maxima). This is obvious as the contribution of long-range Coulomb potential is dominant at the lower scattering angles. However, it starts showing some structures in the DCS results at the intermediate angles due to the effect of the field of atomic electrons. These structures may be also due to overlap (or interference) of incident electron partial

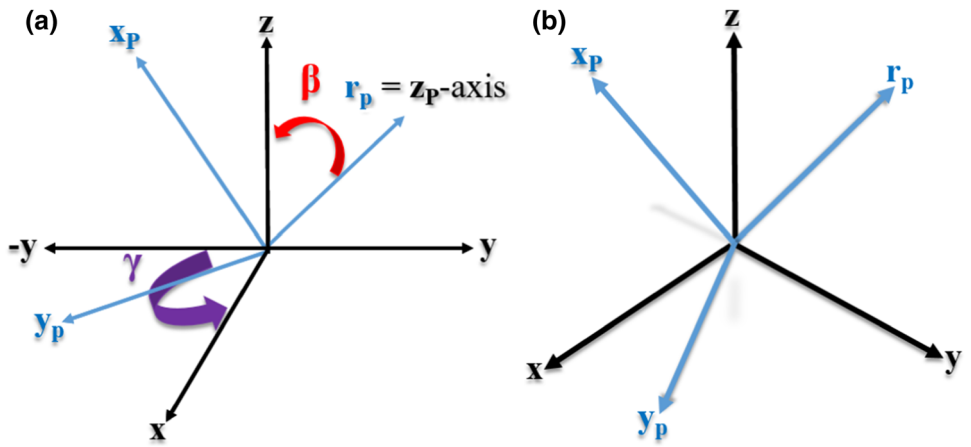

Fig. 1 **a** A diagram showing the rotation Euler angles (α, β, γ) and **b** (x, y, z) are the set of orthogonal vectors with respect to which the Gaussian orbitals are calculated. $\boldsymbol{r}_P$ is the product vector as defined in Eq. (21) while x_p is an arbitrary vector perpendicular to $\boldsymbol{r}_P$ and y_p is perpendicular to both $\boldsymbol{r}_P$ and x_p. (α, β, γ) are the standard Euler angles needed to rotate $(x_p, y_p, \boldsymbol{r}_P)$ to (x, y, z)

Table 10 Calculated Euler angles (α, β, γ) of CH_4^+, NH_3^+, H_2O^+, NH_4^+ and H_3O^+ molecular ions

	α	β	γ
CH_4^+			
C–H1	0.0000	$\cos^{-1}(0.4749)$	$\pi/2$
C–H2	0.0000	$\cos^{-1}(0.4749)$	$3\pi/2$
C–H3	0.0000	$\pi - \cos^{-1}(0.8732)$	π
C–H4	0.0000	$\pi - \cos^{-1}(0.8732)$	0.0000
H1–H2	0.0000	0.0000	0.0000
H1–H3	0.0000	$\pi - \cos^{-1}(0.4217)$	$\pi - \cos^{-1}(0.5174)$
H1–H4	0.0000	$\pi - \cos^{-1}(0.4217)$	$\cos^{-1}(0.5174)$
H2–H3	0.0000	$\pi - \cos^{-1}(0.4217)$	$\pi + \cos^{-1}(0.5174)$
H2–H4	0.0000	$\pi - \cos^{-1}(0.4217)$	$2\pi - \cos^{-1}(0.5174)$
H3–H4	0.0000	π	$\pi/2$
NH_3^+			
N–H1	0.0000	0.0000	0.0000
N–H2	0.0000	0.0000	$\pi - \cos^{-1}(0.8660)$
N–H3	0.0000	0.0000	$\cos^{-1}(0.8660)$
H1–H2	0.0000	0.0000	$\pi + \cos^{-1}(0.8660)$
H1–H3	0.0000	0.0000	$2\pi - \cos^{-1}(0.8660)$
H2–H3	0.0000	$\pi/2$	$3\pi/2$
H_2O^+			
O–H1	0.0000	$\pi - \cos^{-1}(0.5757)$	$\pi/2$
O–H2	0.0000	$\pi - \cos^{-1}(0.5757)$	$3\pi/2$
H1–H2	0.0000	π	$\pi/2$
NH_4^+			
N–H1	0.0000	$\cos^{-1}(1/\sqrt{3})$	$3\pi/4$
N–H2	0.0000	$\cos^{-1}(1/\sqrt{3})$	$7\pi/4$
N–H3	0.0000	$\pi - \cos^{-1}(1/\sqrt{3})$	$\pi/4$
N–H4	0.0000	$\pi - \cos^{-1}(1/\sqrt{3})$	$5\pi/4$
H1–H2	0.0000	$\pi/2$	π
H1–H3	0.0000	$\pi/2$	$\pi/2$
H1–H4	0.0000	0.0000	0.0000
H2–H3	0.0000	π	$\pi/2$
H2–H4	0.0000	$\pi/2$	$3\pi/2$
H3–H4	0.0000	$\pi/2$	0.0000
H_3O^+			
O–H1	0.0000	$\pi - \cos^{-1}(0.2731)$	$\pi/2$
O–H2	0.0000	$\pi - \cos^{-1}(0.2731)$	$2\pi - \cos^{-1}(0.8660)$
O–H3	0.0000	$\pi - \cos^{-1}(0.2731)$	$\pi + \cos^{-1}(0.8660)$
H1–H2	0.0000	$\pi - \cos^{-1}(0.4938)$	$\cos^{-1}(0.8660)$
H1–H3	0.0000	$\pi - \cos^{-1}(0.4938)$	$3\pi/2$
H2–H3	0.0000	$\pi - \cos^{-1}(0.4938)$	$\pi - \cos^{-1}(0.8660)$

waves. We observed a general feature that as the incident electron energy increases, the structure in the DCS curves starts disappearing and the magnitude of the cross section decreases. Also with the increasing energy, the minima of the DCS curves get shifted toward the lower scattering angles and the interference structures also become flatter. In Fig. 3b, we have shown the DCS results for 100–500 eV incident electron energies and we see that the DCS curves fall off monotonically with the increasing scattering angles. At such high incident electron energies, for the backscattering angles, the DCS curves do not show any maxima or minima but the magnitude of the DCS decreases slowly as the incident electron energy increases. It is obvious as the incident electron energy increases, the probability of interaction between the electron and the target ion becomes less and it just passes away.

We have shown in Fig. 4a–d, the comparison of the DCS results for electron scattering from CH_4^+ molecular ion with its neutral molecule CH_4 at various incident electron energies viz. 20, 50, 100 and 500 eV. In these figures, electron scattering from pure Coulomb ionic charge of the CH_4^+ molecular ion are also included for comparison. From these figures, we observe that the general behavior of cross sections of CH_4^+ molecular ion and neutral CH_4 molecule is quite similar. We also see in the near forward scattering angles, the DCS for CH_4^+ is higher than CH_4 and thereafter at backward angles attain almost the same magnitude. This may be due to the additional effect of the Coulomb potential in the

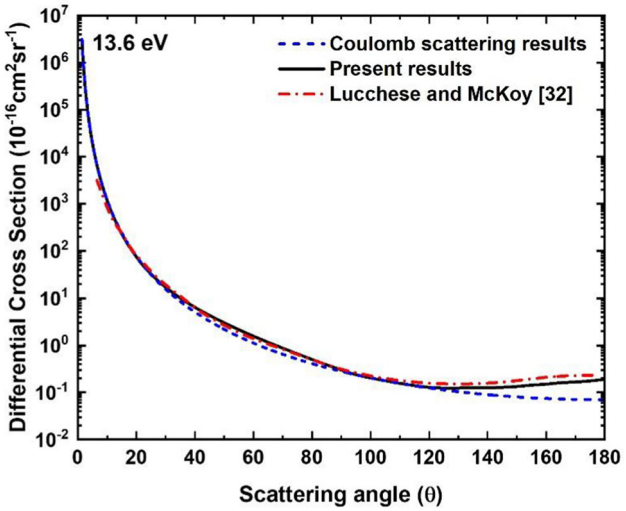

Fig. 2 Differential cross section for electron–H_2^+ scattering at incident electron energy 13.6 eV

case of CH_4^+ molecular ion. The behavior of the pure Coulomb scattering is the same as we explained in Fig. 2 for H_2^+, i.e., the Coulomb potential dominates in the forward scattering angles whose contribution slightly differs at different incident electron energies and thereafter, short-range part of the potential contributes.

3.2 DCS results for electron–NH_3^+ scattering

In Fig. 5, we have shown the DCS results for electron scattering from NH_3^+ molecular ion in the 10–500 eV incident electron energy range. Our DCS results for NH_3^+ molecular ion in the 10–50 eV energy range is shown in Fig. 5a. We can see a similar trend of DCS behavior as for CH_4^+ molecular ion, though with a different magnitude of the DCS values and the associated interference structure. From Fig. 5a, we see a prominent minimum occurring at incident electron energies of 10 and 20 eV and as the energy increases, the minimum position is shifted toward the lower scattering angles and disappears at higher energies. We have also shown the DCS results at 100–500 eV incident electron energies in Fig. 5b. The cross sections fall off as the energy increases and after a certain angle, especially toward the backscattering angle, the cross section does not significantly change with the scattering angles.

Comparison of the DCS curves for electron scattering from NH_3^+ molecular ion is made with its neutral NH_3 molecule as shown in Fig. 6a–d. The electron scattering results from the pure Coulomb ionic charge of the NH_3^+ molecular ion are also included for comparison. We observe that the main difference in the two sets of DCS results can be noticed only in the near forward and intermediate scattering angles and at relatively lower incident energies. As energy increases, both the results tend to merge. The behavior of the comparison with respect to the Coulomb scattering is similar as seen in Fig. 4.

3.3 DCS results for electron–H_2O^+ scattering

We have shown the DCS results for electron–H_2O^+ at 10–500 eV incident electron energies in Fig. 7. We observe from this figure, at 10 eV, a prominent minimum position at 118° scattering angle and as the energy increased further, the DCS curves do not show such feature, although some slight structure can be seen. We have shown the DCS results for 100–500 eV incident electron energies in Fig. 7b and find the similar behavior as for other molecules considered above.

Figure 8a–d displays the comparison of DCS results for H_2O^+ molecular ion with its parent molecule H_2O. The pure Coulomb scattering results for the H_2O^+ molecular ion are also included for comparison. We can

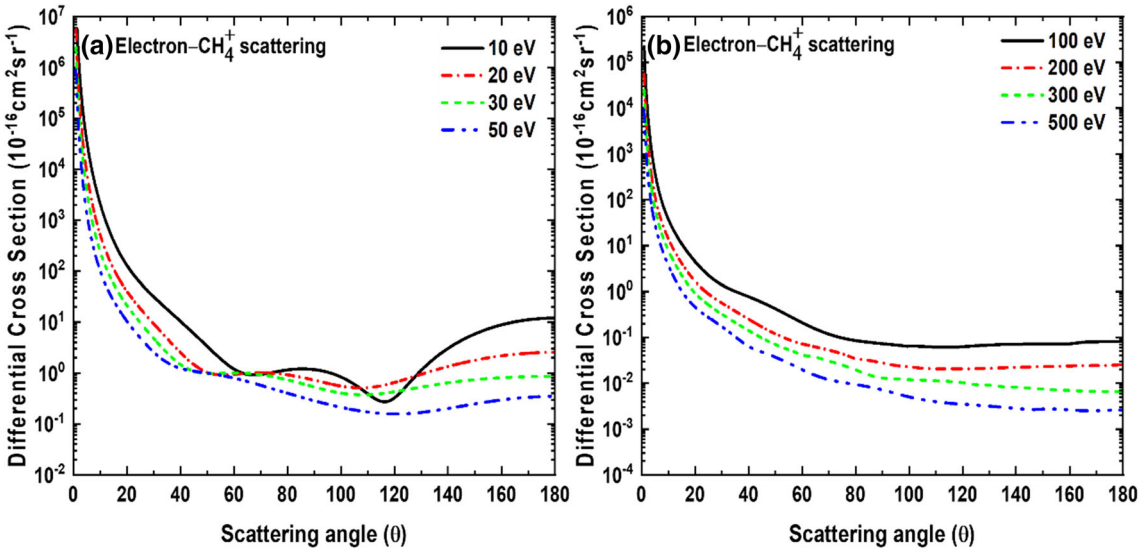

Fig. 3 Differential cross sections for electron–CH_4^+ scattering at incident electron energies **a** 10–50 eV and **b** 100–500 eV

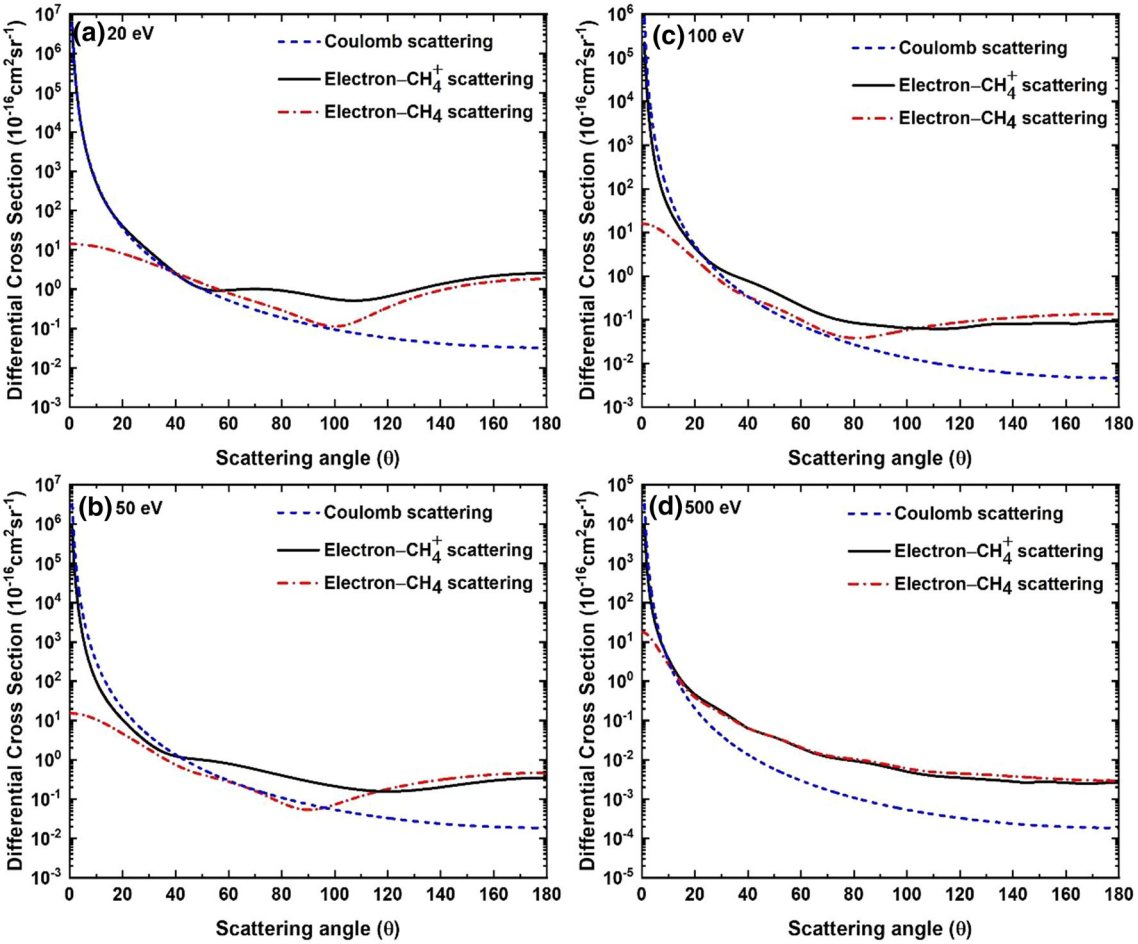

Fig. 4 Comparison of differential cross sections for electron scattering from CH_4^+ and CH_4 at incident electron energies (a) 20 eV, (b) 50 eV, (c) 100 eV and (d) 500 eV

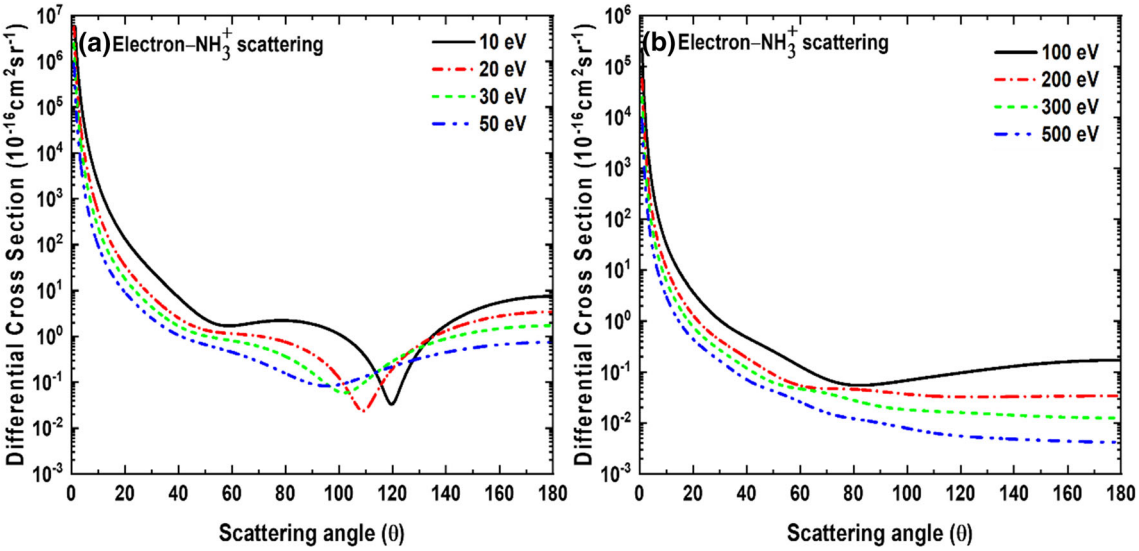

Fig. 5 Differential cross sections for electron–NH_3^+ scattering at incident electron energies **a** 10–50 eV and **b** 100–500 eV

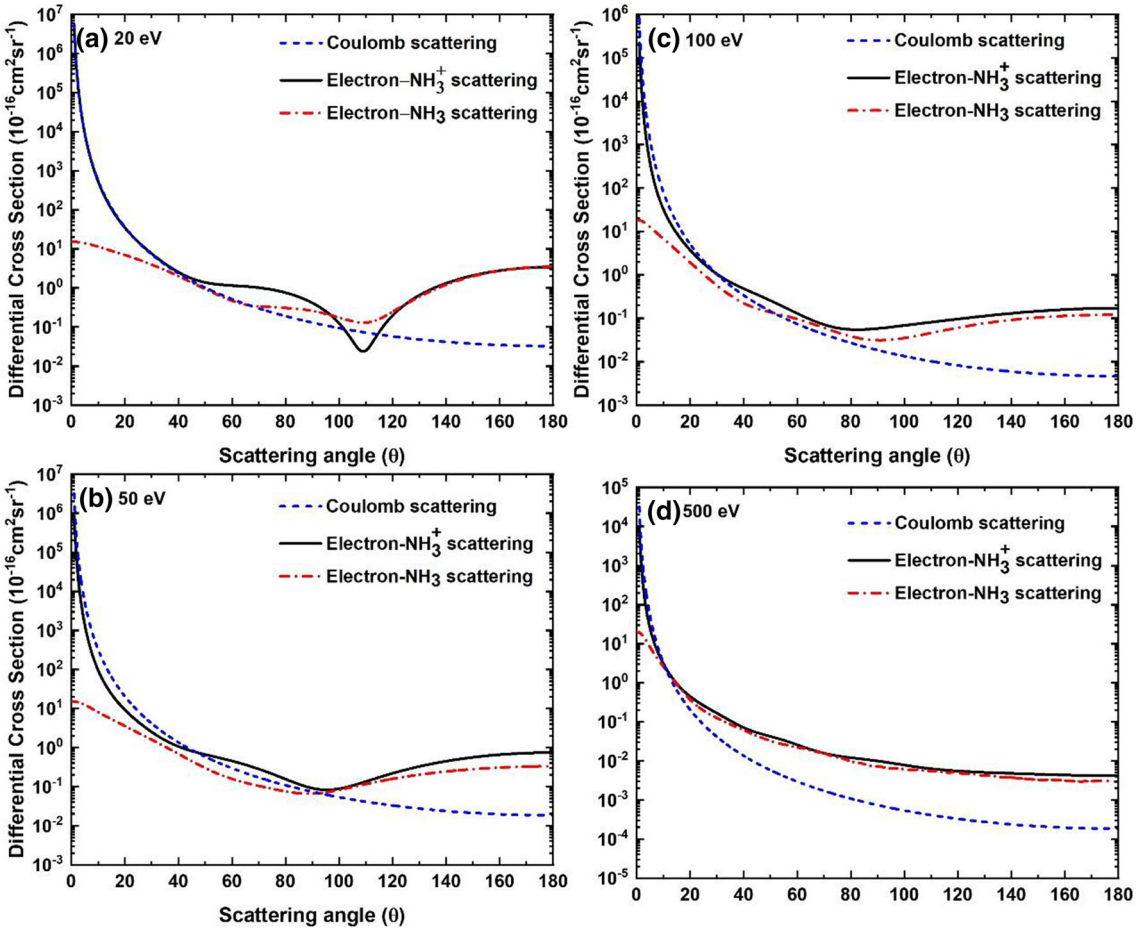

Fig. 6 Comparison of differential cross sections for electron scattering from NH_3^+ and NH_3 at incident electron energies **a** 20 eV, **b** 50 eV, **c** 100 eV and **d** 500 eV

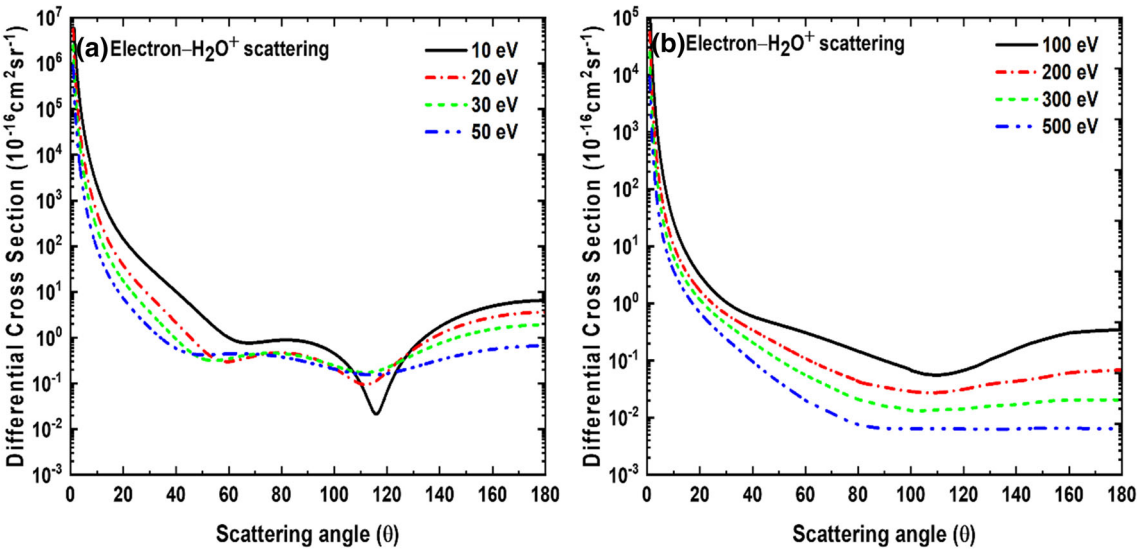

Fig. 7 Differential cross sections for electron–H_2O^+ scattering at incident electron energies **a** 10–50 eV and **b** 100–500 eV

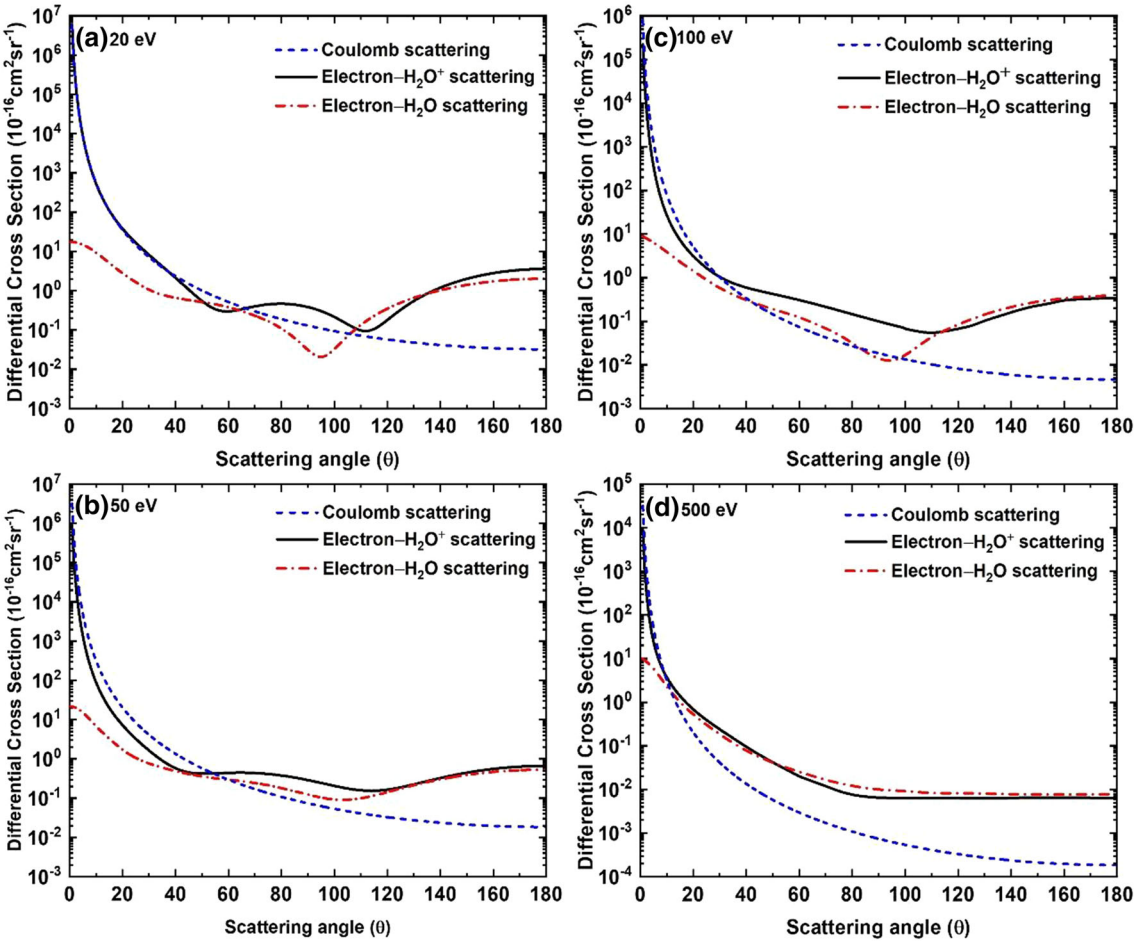

Fig. 8 Comparison of differential cross sections for electron scattering from H_2O^+ and H_2O at incident electron energies **a** 20 eV, **b** 50 eV, **c** 100 eV and **d** 500 eV

see a similar trend as in Figs. 4 and 6. In all the comparisons at different energies, we notice that the DCS structures are different from their parent molecules at lower energies, especially with respect to the position of minimum. This noticeable difference is primarily due to the Coulomb potential and partially, it may be because of their different structural compositions as well as the polarization potential considered where they have different values of the dipole polarizability. As we increase the energy, we find that the DCSs approach the values for their parent molecule above 60° .

3.4 DCS results for electron scattering from NH_4^+ and H_3O^+

Finally, in Figs. 9 and 10, respectively, we have reported DCS results for NH_4^+ and H_3O^+ molecular ions. From these figures, we find that the behavior of cross section curves are quite similar to the results presented for the CH_4^+, NH_3^+, H_2O^+ molecular ions. At lower energies, they show a prominent minimum and the position of the minimum is shifted toward the forward angles as the energy is increased. For higher energies above 100 eV, the DCS curves show flat nature after a sharp fall in the lower scattering angle due to the long-range Coulomb potential.

4 Conclusions

In the present work, we have studied the elastic scattering of electrons from the H_2^+, CH_4^+, NH_3^+, H_2O^+, NH_4^+ and H_3O^+ molecular ions using optical model potential method. To construct the optical potential, we have obtained an analytical static potential from the molecular ionic charge density using the Gaussian wavefunction with STO-6G basis set calculated through the GAUSSIAN-16 software. Further, the exchange and polarization potentials are also added to the static potential to obtain the optical model potential. The Dirac equations are solved using this optical potential with the partial wave technique to get the phase shifts and scattering amplitudes with which the DCS are calculated. The calculation for electron scattering from H_2^+ is presented for the comparison purpose with the previously available theoretical calculation, just to test our theoretical approach. The DCS results are reported for

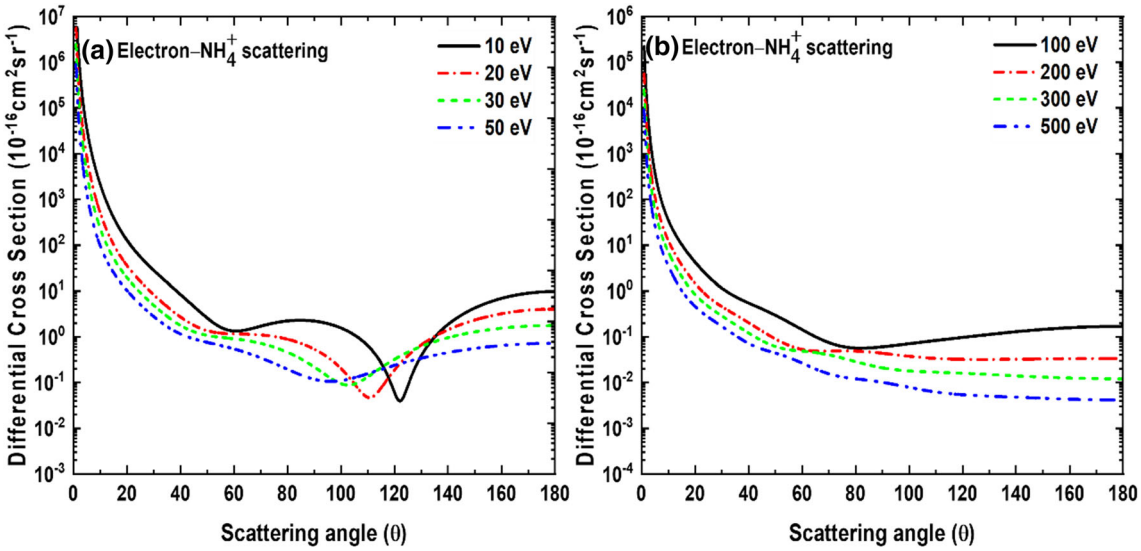

Fig. 9 Differential cross sections for electron–NH_4^+ scattering at incident electron energies **a** 10–50 eV and **b** 100–500 eV

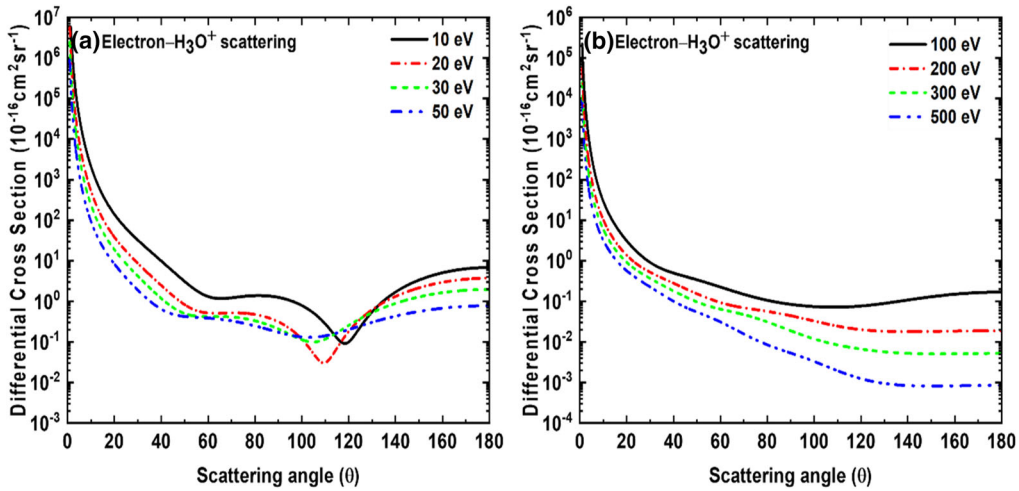

Fig. 10 Differential cross sections for electron–H_3O^+ scattering at incident electron energies **a** 10–50 eV and **b** 100–500 eV

the first time for the elastic electron scattering from the five important CH_4^+, NH_3^+, H_2O^+, NH_4^+ and H_3O^+ molecular ions for the incident electron energies from 10 to 500 eV. As no previous such study has been done on these molecular ions, we have compared our present DCS results with their corresponding neutral molecules which we had previously reported in our earlier work. This provides us an interesting comparison of the electron collision cross sections with a neutral molecule and its ion. We found at low incident electron energies, the DCS–energy curves show noticeably different behaviors for each ion in comparison to the neutral molecules and they have a sharp peak in the forward direction due to the dominant Coulomb potential of the residual charge of the ion. Also as the incident electron energy increases, the behavior of the DCS curves for the different ions tends to be similar to their corresponding neutral molecules. To see the contribution of the Coulomb and short-range potentials, the results for the electron scattering from pure Coulomb ionic charge of the molecular ions are also compared. We find that the Coulomb potential dominates in the forward scattering angles whose contribution slightly differs at different incident electron energies and thereafter short-range part of the potential contributes. We believe our present work will stimulate more research on the collisions of electrons from the molecular ions on account of their many important applications.

Acknowledgements The authors, DM is thankful to the Ministry of Human Resources and Development (MHRD), Govt. of India, and RS and LS are thankful to SERB-DST, New Delhi, Govt. of India for the sanction of research Grant No. CRG/2020/005597.

Author contributions

DM contributed to formal analysis, investigation, methodology, software and writing—original draft. LS contributed to formal analysis, funding acquisition, methodology, supervision and writing—review and editing. RS initiated the original research problem and contributed to formal analysis, funding acquisition, methodology, supervision and writing—review and editing.

Data Availability Statement This manuscript has no associated data or the data will not be deposited. [Authors' comment: The datasets generated during and/or analysed during the current study are available from the corresponding author on reasonable request.]

References

1. D.H. Sampson, H.L. Zhang, C.J. Fontes, Phys. Rep. **477**, 111 (2009)
2. K. Bartschat, M.J. Kushner, Proc. Natl. Acad. Sci. **113**, 7026 (2016)
3. B.A. Huber, C. Ristori, C. Guet, D. Küchler, W.R. Johnson, Phys. Rev. Lett. **73**, 2301 (1994)
4. C. Bélenger, P. Defrance, R. Friedlein, C. Guet, D. Jalabert, M. Maurel, C. Ristori, J.C. Rocco, B.A. Huber, J. Phys. B At. Mol. Opt. Phys. **29**, 4443 (1996)
5. I.D. Williams, B. Srigengan, J.B. Greenwood, W.R. Newell, A. Platzer, L. O'Hagan, Phys. Scr. **T73**, 119 (1997)
6. J.T. Shepherd, A.S. Dickinson, J. Phys. B At. Mol. Opt. Phys. **32**, 513 (1999)
7. S. Micheau, Z. Chen, A.T. Le, J. Rauschenberger, M.F. Kling, C.D. Lin, Phys. Rev. Lett. **102**, 073001 (2009)
8. D. Mahato, L. Sharma, R. Srivastava, Int. J. Quantum Chem. (2021). https://doi.org/10.1002/qua.26815
9. B.M. McLaughlin, C.J. Gillan, P.G. Burke, J.S. Dahler, Nucl. Inst. Methods Phys. Res. B **53**, 518 (1991)
10. Y.K. Kim, K.K. Irikura, M.A. Ali, J. Res. Natl. Inst. Stand. Technol. **105**, 285 (2000)
11. N.G. Adams, V. Poterya, L.M. Babcock, Mass Spectrom. Rev. **25**, 798 (2006)
12. N. Pop, Z. Mezei, O. Motapon, S. Niyonzima, K. Chakrabarti, F. Colboc, R. Boată, M.D.E. Epée, I.F. Schneider, AIP Conf. Proc. **1796**, 020014 (2017)
13. D.A. Little, K. Chakrabarti, J.Z. Mezei, I.F. Schneider, J. Tennyson, Phys. Rev. A **90**, 052705 (2014)
14. M.C. Zammit, D.V. Fursa, I. Bray, Phys. Rev. A **90**, 022711 (2014)
15. L.H. Scarlett, M.C. Zammit, D.V. Fursa, I. Bray, Phys. Rev. A **96**, 022706 (2017)
16. A. Faure, V. Kokoouline, C.H. Greene, J. Tennyson, J. Phys. B At. Mol. Opt. Phys. **39**, 4261 (2006)
17. Z.J. Mezei, K. Chakrabarti, M.D. Epée Epée, O. Motapon, C.H. Yuen, M.A. Ayouz, N. Douguet, S. Fonseca Dos Santos, V. Kokoouline, I.F. Schneider, ACS Earth Sp. Chem. **3**, 2376 (2019)
18. International Atomic Energy Agency, *Atomic and Plasma–Material Interaction Data for Fusion, Atomic and Plasma–Material Interaction Data for Fusion No. 16, IAEA*, Vienna (2014)
19. M. Larsson, W.D. Geppert, G. Nyman, Rep. Progr. Phys. **75**, 066901 (2012)
20. R.K. Janev, D. Reiter, Phys. Plasmas **9**, 4071 (2002)
21. R.D. Thomas, Mass Spectrom. Rev. **27**, 485 (2008)
22. R. Perillo, R. Chandra, G.R.A. Akkermans, W.A.J. Vijvers, W.A.A.D. Graef, I.G.J. Classen, J. van Dijk, M.R. de Baar, Plasma Phys. Control Fus. **60**, 105004 (2018)
23. S. Rednyk, Š Roučka, A. Kovalenko, T.D. Tran, P. Dohnal, R. Plašil, J. Glosík, Astron. Astrophys. **625**, A74 (2019)
24. A. Beth, K. Altwegg, H. Balsiger, J.-J. Berthelier, U. Calmonte, M.R. Combi, J. De Keyser, F. Dhooghe, B. Fiethe, S.A. Fuselier, M. Galand, S. Gasc, T.I. Gombosi, K.C. Hansen, M. Hässig, K.L. Héritier, E. Kopp, L. Le Roy, K.E. Mandt, S. Peroy, M. Rubin, T. Sémon, C.-Y. Tzou, E. Vigren, Mon. Not. R. Astron. Soc. **462**, S562 (2017)
25. Cooling Water, https://www.iter.org/mach/Coolingwater
26. P.A. Wehinger, S. Wyckoee, G.H. Herbig, G. Herzberg, H. Lew, Astrophys. J. **190**, L43 (1974)
27. A. Wootten, F. Boulanger, M. Bogey, F. Combes, P.J. Encrenaz, M. Gerin, L. Ziurys, Philos. Trans. R. Soc. Lond. Ser. A, Math. Phys. Sci. **303**, 543 (1981)
28. V. Laporta, K. Chakrabarti, R. Celiberto, R.K. Janev, J.Z. Mezei, S. Niyonzima, J. Tennyson, I.F. Schneider, Plasma Phys. Control. Fusion **59**(2017)
29. A. Abdoulanziz, C. Argentin, V. Laporta, K. Chakrabarti, A. Bultel, J. Tennyson, I.F. Schneider, J.Z. Mezei, J. Appl. Phys. **129** (2021)
30. R.R. Lucchese, V. McKoy, Phys. Rev. A **21**, 112 (1980)
31. R.R. Lucchese, V. McKoy, Phys. Scr. **21**, 366 (1980)
32. R.R. Lucchese, V. McKoy, Phys. Rev. A **24**, 770 (1981)
33. D. Mahato, L. Sharma, A.D. Stauffer, R. Srivastava, Eur. Phys. J. D **73**, 189 (2019)
34. D. Mahato, L. Sharma, R. Srivastava, J. Phys. B At. Mol. Opt. Phys. **53**, 225204 (2020)
35. D. Mahato, L. Sharma, R. Srivastava, J. Electron Spectros. Relat. Phenomena **252**, 147118 (2021)
36. D. Mahato, L. Sharma, R. Srivastava, Atoms **8**, 83 (2020)
37. F. Salvat, Phys. Rev. A **68**, 012708 (2003)
38. F. Salvat, A. Jablonski, C.J. Powell, Comput. Phys. Commun. **165**, 157 (2005)
39. L. Sharma, A. Surzhykov, R. Srivastava, S. Fritzsche, Phys. Rev. A **83**, 062701 (2011)
40. T. Das, A.D. Stauffer, R. Srivastava, Eur. Phys. J. D **68**, 102 (2014)
41. I. Tóth, R.I. Campeanu, V. Chiş, L. Nagy, Phys. Lett. A **360**, 131 (2006)
42. I. Tóth, R.I. Campeanu, L. Nagy, Eur. Phys. J. D **69**, 2 (2015)
43. J.B. Furness, I.E. McCarthy, J. Phys. B At. Mol. Phys. **6**, 2280 (1973)